Supporting Information

for

Insights into Degradation of Metallic Lithium Electrode Protected by Bilayer Solid Electrolyte Based on Aluminium Substituted Lithium Lanthanum Titanate in Lithium-Air Batteries

Hang T. T. Le,[a] Duc Tung Ngo,[a] Van-Chuong Ho,[a] Guozhong Cao,[b] and Chan-Jin Park [a,]*

[a] Department of Materials Science and Engineering, Chonnam National University, 77, Yongbongro, Bukgu, Gwangju 500-757, South Korea

[b] Department of Materials Science and Engineering, University of Washington, Seattle, WA 98195-2120, United States

* Corresponding author.

Tel.: +82-62-530-1704;

Fax: +82-62-530-1699

E-mail address: parkcj@jnu.ac.kr (C.J. Park)

Tab. S1. Binding energies corresponding to the fitted peaks for the surface of the Li electrode of the Li-air cell.

Components	Binding energy (eV)				
	C1s	O1s	F1s	$S2p_{3/2}$	N1s
Hydrocarbon	285				
LiTFSI	292.6		688.5	168.7	399.4
Li_2O		528.8			
LiF			684.9		
Li_3N					397
Li_2S				161.2	
$Li_2S_2O_4$				166.2	
Li_2SO_3				167.6	
Polysulfur				163.8	
Li_2CO_3	290.3	531.8			
-COO	287-288	532.3			
C-O	286.1-287.1	533.6			

Tab. S2. Fitted parameters corresponding to equivalent circuit models for the impedance of the MnO_2@Ni air electrode, before and after 20 cycles of discharge-charge test in pure oxygen atmosphere and in air atmosphere.

Sample	R_e (Ω)	R_f (Ω)	CPE_f		R_{ct} (Ω)	CPE_{dl}		CPE_{dif}	
			C_f (F)	n_f		C_{dl} (F)	n_{dl}	C_{dif} (F)	n_{dif}
Before test	8.6	-	-	-	83.3	1.97×10^{-5}	0.804	1.39×10^{-2}	0.813
After test in O_2	8.9	30.2	5.10×10^{-4}	0.542	94.0	1.72×10^{-5}	0.898	1.96×10^{-2}	0.709
After test in air	10.2	87.0	4.73×10^{-3}	0.792	298.3	1.62×10^{-5}	0.771	3.33×10^{-3}	0.705

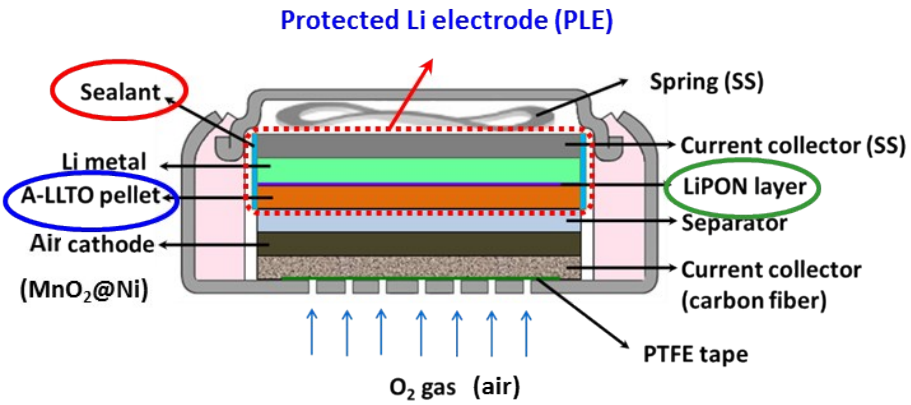

Fig. S1. Configuration of the modified coin-type Li-air cell employing the LiPON/A-LLTO bilayer solid electrolyte.

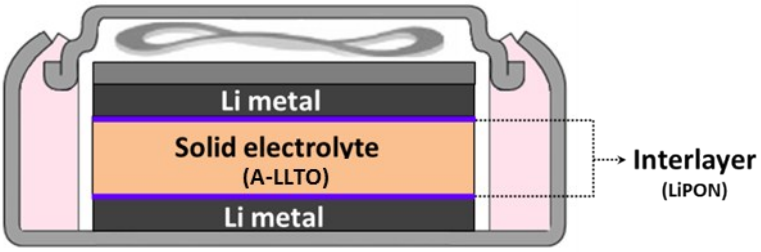

Fig. S2. Symmetric cell composed of Li/LiPON/A-LLTO/LiPON/Li.

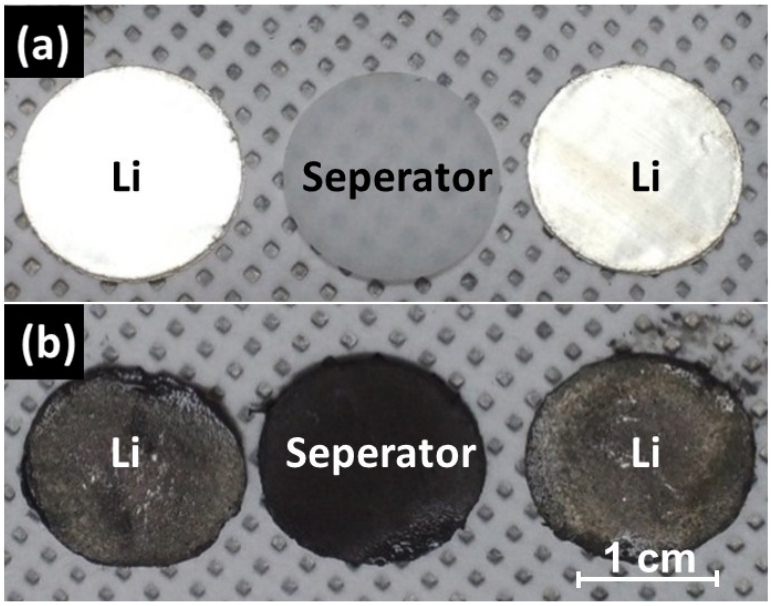

Fig. S3. Typical images of components from the symmetric cell of Li/Separator/Li; (a) before and (b) after the galvanostatic cycling test under the limited capacity mode of 1 mAh cm^{-2} at the current density of 0.5 mA cm^{-2}.

In order to further confirm the formation of what is known as the "dead Li dendrites", the symmetric cell after the cycling test was disassembled for observation. As shown in **Fig. S3**a, before the test, the Li electrode showed the typical bright white colour of Li metal. The pristine separator was translucent. After 15 cycles of charge-discharge under the limited capacity mode at the current density of 0.5 mA cm^{-2}, the colour of the surface of the Li electrode and separator changed from white to grey (**Fig. S3**b). This illustrates the formation of Li dendrites on the surface of the Li electrode and the formation of dead Li dendrites, which were entangled in the separator and changed the colour of the separator. The dead Li dendrites trapped in the separator are shown more clearly in **Fig. S4**. Herein, the difference between the SEM images of the separator before and after the cycling test is clear. Before cycling, the separator was composed of many fibers with a diameter ranging from 200 nm to 1 μm (**Fig. S4**a). During charging process, the Li dendrites grew into void spaces among the glass fibers. Further, during the discharging process, the Li dendrites were partly stripped to leave behind the dead Li dendrites embedded in the separator as shown in **Fig. S4**b.

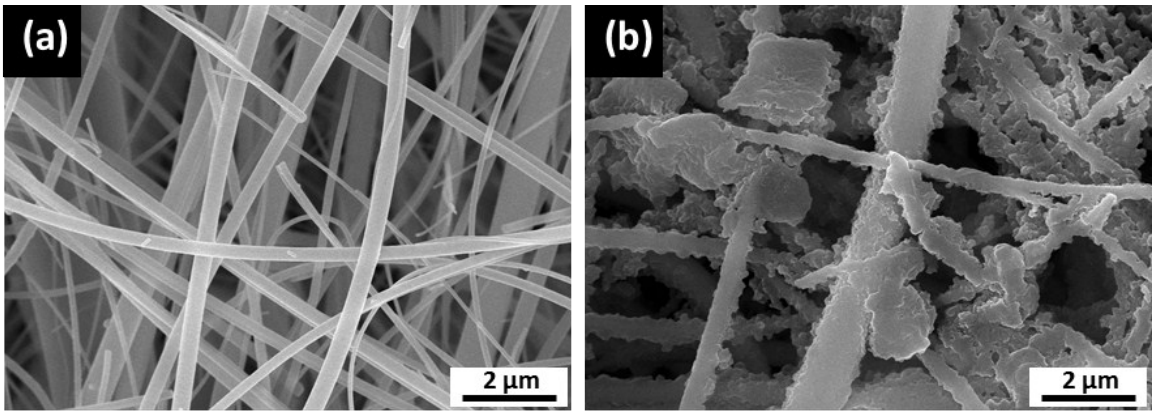

Fig. S4. SEM images of glass fiber separator; (a) pristine and (b) after the cell's failure in the cycling test under the limited capacity mode of 1 mAh cm^{-2} at the current density of 0.5 mA cm^{-2}.

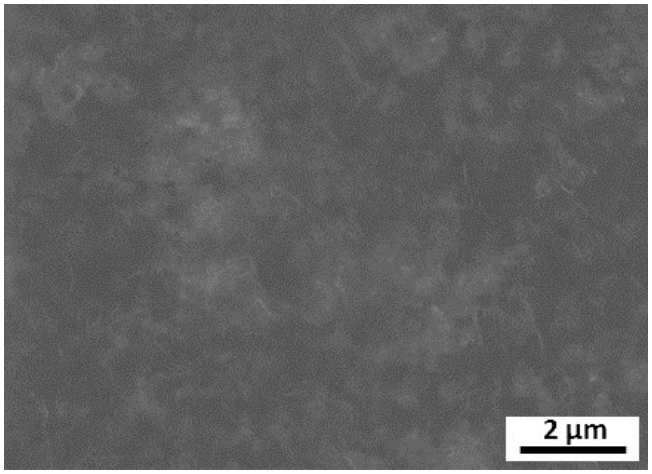

Fig. S5. SEM image of the pristine Li metal electrode before the cyclic test.

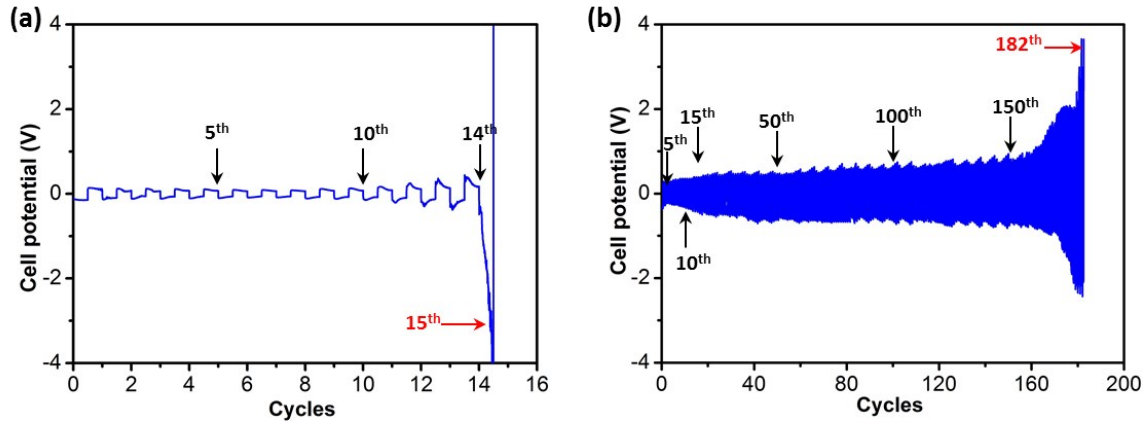

Fig. S6. Cell potential profiles of the symmetric cell of (a) Li/Separator/Li and (b) Li/LiPON/A-LLTO/LiPON/Li cycled under the limited capacity of 1 mAh cm^{-2} at the current density of 0.5 mA cm^{-2}.

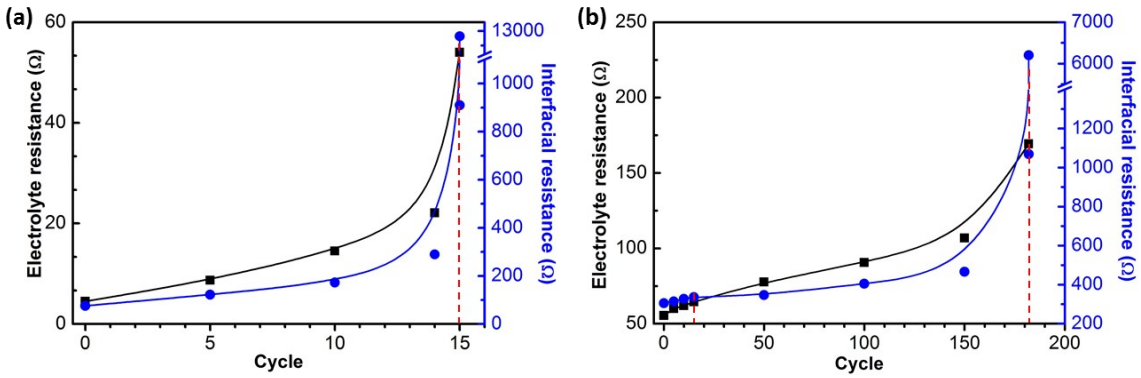

Fig. S7. Variation of electrolyte resistance and interfacial resistance with cycle for the symmetric cells of (a) Li/Separator/Li and (b) Li/LiPON/A-LLTO/LiPON/Li cycled under the limited capacity mode of 1 mAh cm^{-2} at the applied current density of 0.5 mA cm^{-2}.

To show the definite effect of the solid electrolyte on the interfacial electrochemistry of the Li electrode during the cycling process, the variation of electrolyte resistance and interfacial resistance with the cycle for the symmetric cells with and without LiPON/A-LLTO, which was obtained from the corresponding Nyquist plots (**Fig. 7**), is shown in **Fig. S7**. In **Fig. 7**, the shape of the Nyquist plots is simple, almost forming a semicircle. The intersections on the Z' axis at high frequency range and low frequency range correspond to the electrolyte resistance and the total resistance composed of the electrolyte resistance and interfacial resistance, respectively. Accordingly, the electrolyte resistance and the interfacial resistance can be easily determined. As shown in **Fig. S7**, after 15 cycles of charge-discharge, the symmetric cell without the solid electrolyte revealed a significant increase in both the electrolyte and interfacial resistance. In particular, the interfacial resistance dramatically increased up to 13 kΩ in the 15^{th} cycle. This result demonstrates that the Li electrode was almost blocked, leading to failure of the cell. In contrast, the interfacial resistance of the symmetric cell employing the solid electrolyte was still quite small (~340 Ω) even after 15 cycles. Further, after 182 cycles, the symmetric cell failed when the interfacial resistance reached 6.2 kΩ.

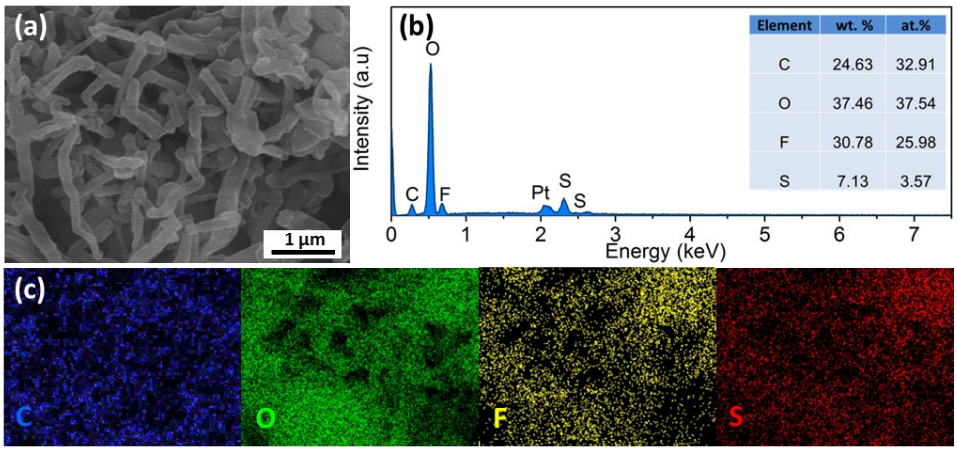

Fig. S8. Analysis of Li electrode detached from the symmetric cell of Li/Separator/Li after the cell's failure in the 15th cycle, when the cell was cycled under the limited capacity mode of 1 mAh cm^{-2} at the current density of 0.5 mA cm^{-2}. (a) SEM image; (b) EDS spectrum and table of relevant elemental composition; (c) EDS elemental mapping for C, O, F, and S.

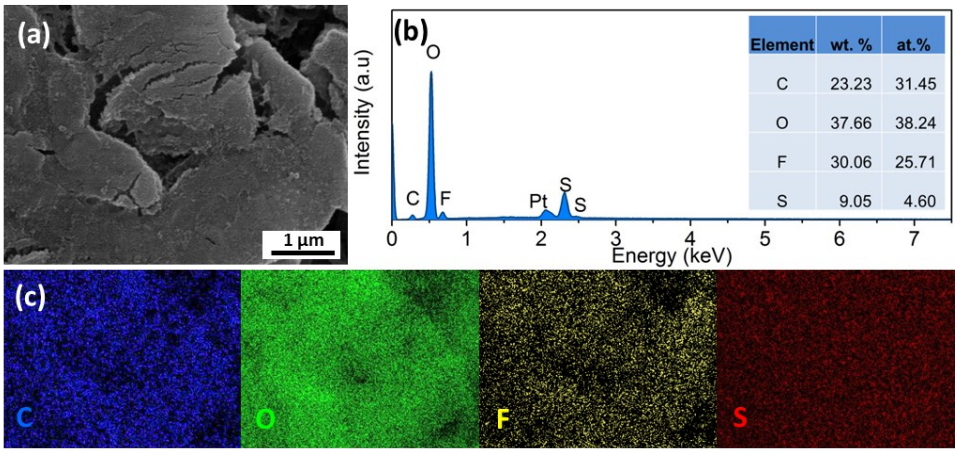

Fig. S9. Li electrode detached from the symmetric cell of Li/LiPON/A-LLTO/LiPON/Li after the cell's failure in the 182th cycle, when the cell was cycled under the limited capacity mode of 1 mAh cm^{-2} at the current density of 0.5 mA cm^{-2}. (a) SEM image; (b) EDS spectrum and table of relevant elemental composition; (c) EDS elemental mapping for C, O, F, and S.

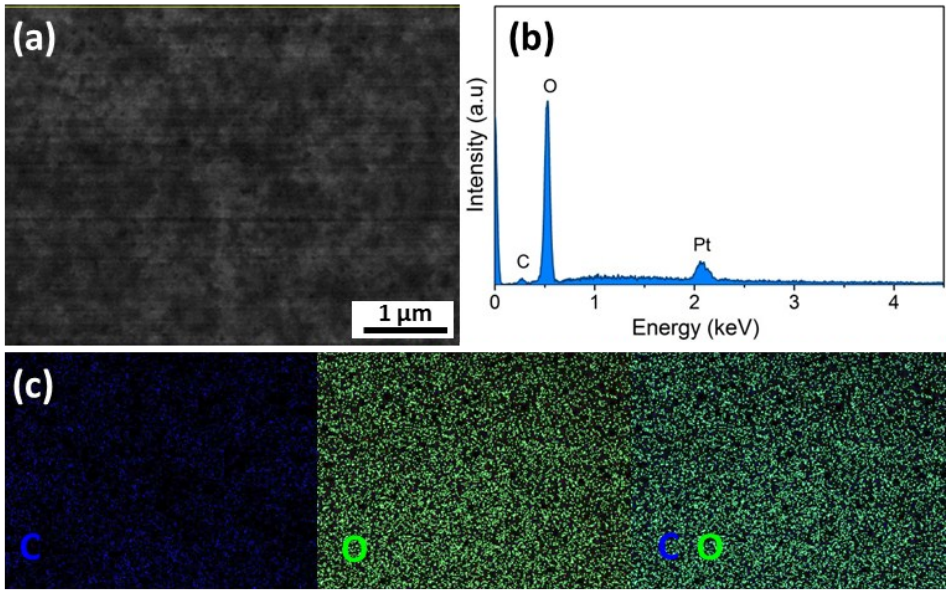

Fig. S10. Pristine Li metal electrode; (a) SEM image, (b) EDS spectrum, and (c) elemental mapping.

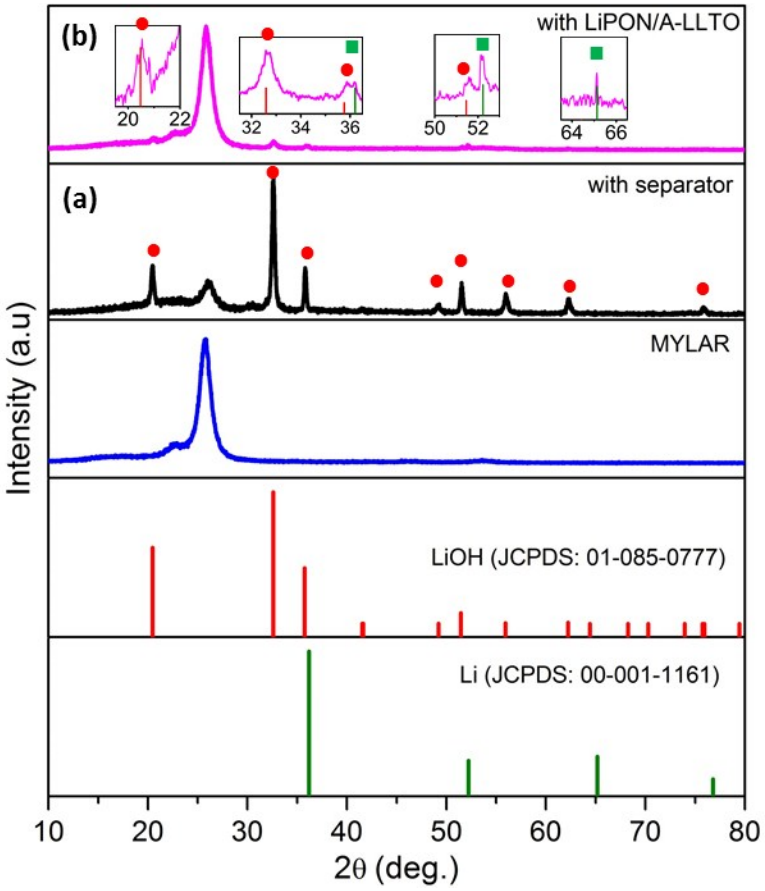

Fig. S11. XRD patterns for the Li electrodes detached from the Li-air cells (a) without and (b) with the LiPON/A-LLTO solid electrolyte after cyclic test in air atmosphere under the limited capacity mode of 1000 mAh g^{-1} at the current density of 0.1 mA cm^{-2}. XRD patterns for Li (■), LiOH (●), and MYLAR X-ray film are also shown as references.

To confirm the change in the nature of the Li electrodes with and without the protection of the LiPON/A-LLTO after the cyclic test in air atmosphere at the current density of 0.1 mA cm^{-2}, the tested Li electrodes were detached from the Li-air cells after the tests and characterized using XRD. In particular, to avoid the unexpected spontaneous oxidation and moisture-adsorption on the Li electrodes during XRD analysis, the tested Li electrodes were carefully protected by the argon air-tight sample holder employing the MYLAR X-ray film.[1-2] As shown in **Fig. S11**a, all observed characteristic XRD peaks for the tested Li electrode without LiPON/A-LLTO were well matched to the peaks corresponding to LiOH (JCPDS card No. 01-085-0777). This result confirmed the transformation of the Li metal electrode into the LiOH compound after the test in

air atmosphere for the cell without the protection of the LiPON/A-LLTO solid electrolyte. In contrast, the characteristic peaks corresponding to Li metal (JCPDS card No. 00-001-1161) remained, except for the extra peaks corresponding to the MYLAR film and LiOH as shown in **Fig. S11**b. This result indicates the maintenance of the metallic nature for the PLE with the protection of the LiPON/A-LLTO, even after the cyclic test in air atmosphere. Herein, the diffraction signal corresponding to Li metal for the PLE was relatively weak due to the light mass of the Li metal active material. The generation of the LiOH compound was unavoidable, even for the PLE. Nevertheless, the relative amount of LiOH for the PLE was found to be much smaller than that for the Li electrode without the protection of the solid electrolyte. The appearance of LiOH on the surface of the Li electrode can be attributed to the trace of H_2O in the TEGDEM solvent, which can react with Li metal to generate LiOH. This is also coincident with the obtained FTIR data shown in **Fig. 11**b.

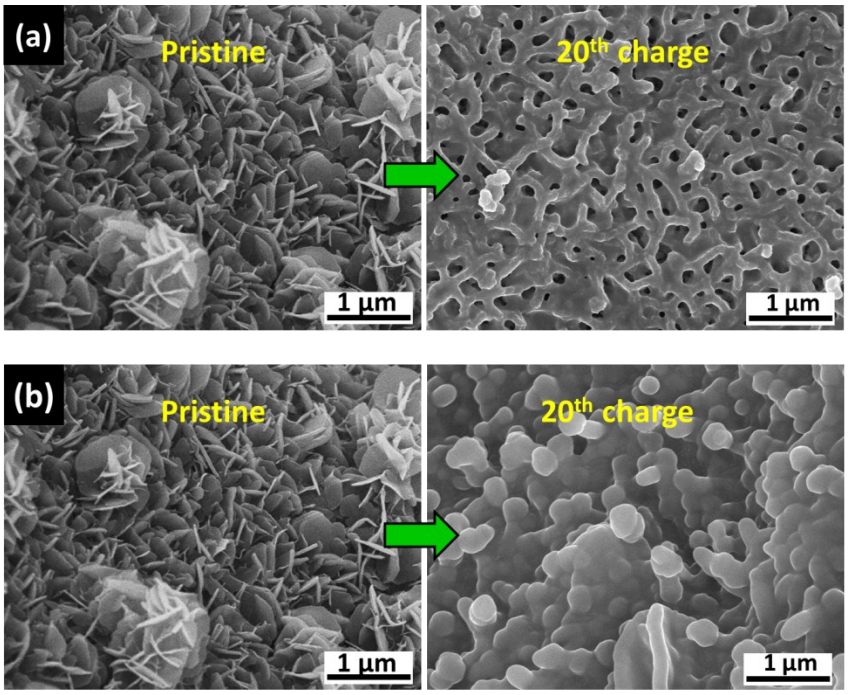

Fig. S12. SEM images of MnO_2@Ni based cathode in Li-air cells employing the PLE before and after 20 cycles of the discharge-charge in the limited capacity mode of 1000 mAh g^{-1} in (a) pure oxygen and (b) air atmosphere.

Fig. S12 shows the effect of the type of gas atmosphere on the surface morphology of the MnO_2@Ni electrode in the Li-air cells employing the PLE after cycling tests. On the whole, the surface of the MnO_2@Ni electrode was almost covered with the reaction products, even after the 20 cycles of the charge process, indicating the degradation of the MnO_2@Ni cathode in both Li-air cells employing the PLE when operated in pure oxygen and air atmosphere. Nevertheless, the cathode cycled in air exhibited more serious deterioration by having a thicker and fuller coverage of reaction products compared with the cathode cycled in pure oxygen.

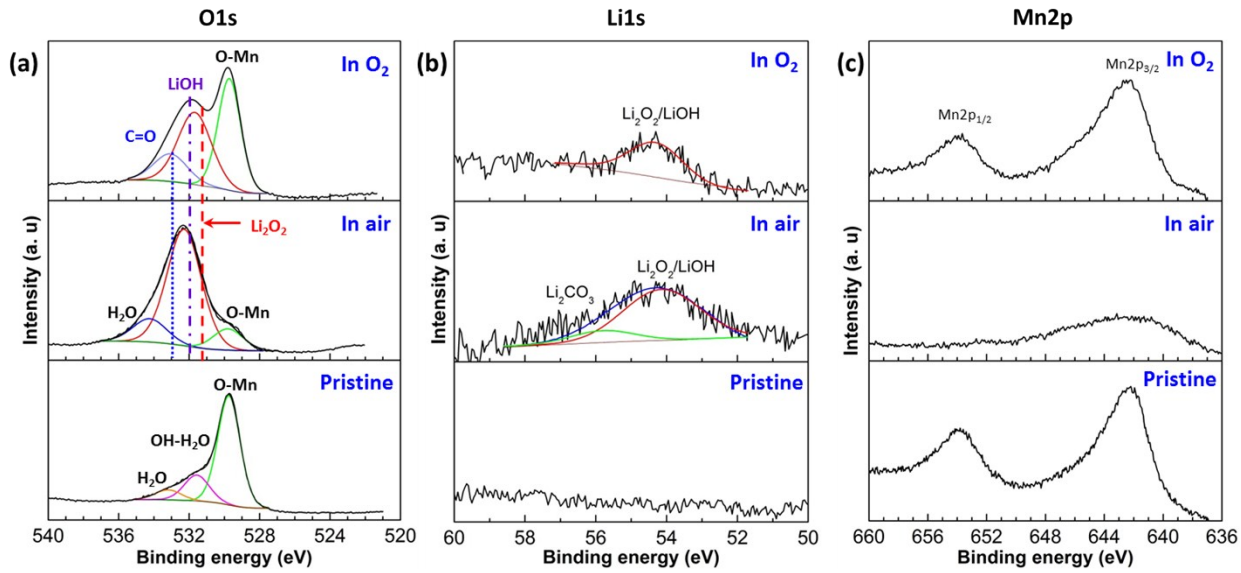

Fig. S13. XPS spectra corresponding to (a) O1s, (b) Li1s, and (c) Mn2p on MnO_2@Ni based cathode detached from the Li-air cell employing the PLE before and after 20 cycles of the discharge-charge test in pure oxygen and air atmosphere under the limited capacity mode of 1000 mAh g^{-1}.

To identify the presence of the reaction products on the MnO_2@Ni electrode after the cycling test, the electrodes were analysed by XPS. As shown in **Figs. S13**a and **S13**c, the sharp peaks observed at 642.2 and 529.7 eV, corresponding to the Mn2p3/2 and O1s spectra, confirmed the 4+ oxidation state of pristine MnO_2@Ni electrode. Unfortunately, typical XPS peaks for the pristine cathode virtually disappeared after 20 cycles of charge-discharge. Instead, the appearance of relevant peaks corresponding to reaction products such as Li_2O_2, LiOH, and Li_2CO_3 was observed. A similar phenomenon was also found for the cathode tested in pure oxygen atmosphere. However, the characteristic peaks for the pristine cathode herein appeared clearly and dominated the other peaks. This implies the partial coverage of the reaction products on the surface of the cathode tested in pure oxygen atmosphere, which is well coincident with the SEM images shown in **Fig. S12**a.

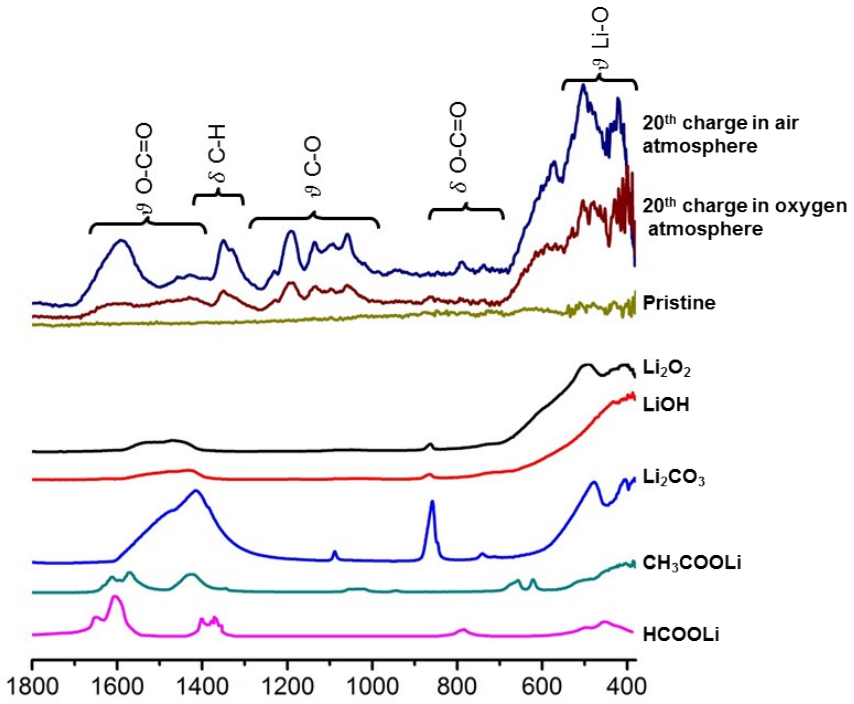

Fig. S14. FTIR spectra for MnO_2@Ni based cathodes detached from the Li-air cells employing the PLE; the pristine electrode and the electrode after test for 20 cycles in pure oxygen and air atmosphere under the limited capacity mode of 1000 mAh g^{-1}.

FTIR was used to further confirm the nature of the surface products after 20 discharge-charge cycles. The FTIR spectra corresponding to Li_2O_2, LiOH, Li_2CO_3, CH_3COOLi, and HCOOLi are presented for comparison. As shown in **Fig. S14**, no peak appeared in the FTIR spectrum for the pristine cathode. After 20 cycles of discharge-charge, the typical peaks corresponding to the groups such as -COO, C-H, C-O, and Li-O showing the presence of Li_2O_2, LiOH, Li_2CO_3, CH_3COOLi, and HCOOLi were found.[3] It is evident that the peaks corresponding to the C-O group, which were detected at the broad wavenumber range from 980 to 1245 cm^{-1}, were derived from the decomposition of the TEGDME solvent on the air electrode surface during the cell operation.[4] Compared with the electrode tested O_2 atmosphere, the electrode tested in air exhibited a much stronger surface absorption, as confirmed in the FTIR spectra within the same test time. This result confirmed the presence of the larger amount of reaction products on the cathode when operated in air atmosphere. This is also the reason why, even when employing the PLE, the Li-air cell suffered from serious degradation when operated in air atmosphere.

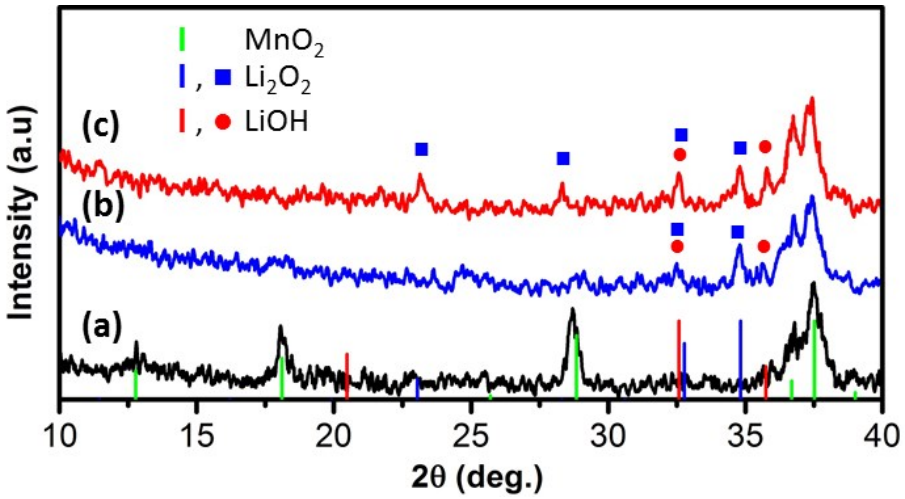

Fig. S15. XRD patterns for MnO_2@Ni foam based cathode detached from the Li-air cells employing the PLE: (a) pristine electrode; electrodes after test for 20 cycles in (b) pure oxygen and (c) air atmosphere.

Fig. S15 shows the clear presence of each LiOH (JCPDS card No. 01-085-1064) and Li_2O_2 (JCPDS card No. 01-073-1640) reaction products on the tested cathode, which was difficult to identify in the XPS data. In particular, for the electrode tested in air atmosphere, all the peaks corresponding to LiOH and Li_2O_2 exhibited a stronger intensity than those for the electrode tested in pure O_2 atmosphere. This demonstrates the larger amount of reaction products on the surface of the tested cathode in air atmosphere, which is in strong agreement with the former obtained XPS and FTIR results.

References

1. M. G. Chourashiya, Y.-H. Kim, C.-N. Park and C.-J. Park, . *J. Alloys Compd.*, 2014, **584**, 47-55.
2. H. T. T. Le, R. S. Kalubarme, D. T. Ngo, S.-Y. Jang, K.-N. Jung, K.-H. Shin and C.-J. Park, *J. Power Sources*, 2015, **274**, 1188-1199.
3. S. A. Freunberger, Y. Chen, N. E. Drewett, L. J. Hardwick, F. Bardé and P. G. Bruce, *Angew. Chem. Int. Ed.*, 2011, **50**, 8609-8613.
4. D. Aurbach, A. Zaban, Y. Ein-Eli, I. Weissman, O. Chusid, B. Markovsky, M. Levi, E. Levi, A. Schechter and E. Granot, *J. Power Sources*, 1997, **68**, 91-98.